Water Quality Assessment of Dye Wastewater after Photocatalytic Treatment with Reduced Graphene Oxide–Metal Oxide Nanocomposites

Roopa M C., Sharadadevi Kallimani*., Umadevi K M., Shilpa P Raikar

Department of Studies in Environmental Science, Davangere University, Davangere, Karnataka 577004, India

***Corresponding Author**

DOI: https://doi.org/10.51584/IJRIAS.2026.11070121

Received: 16 July 2026; Accepted: 21 July 2026; Published: 08 August 2026

ABSTRACT

Textile dyeing effluents remain among the most persistent categories of industrial wastewater owing to their intense color, complex aromatic structures, and resistance to conventional biological treatment. This study reports the post-treatment physicochemical assessment of two structurally distinct textile dyes, the cationic triarylmethane dye Methyl Violet (MV) and the anionic xanthene dye Rose Bengal (RB), following batch photocatalytic treatment with four reduced graphene oxide (rGO)–metal oxide nanocomposites: rGO–CeO_2, rGO–CuO, rGO–MnO_2, and rGO–ZnO. Untreated (baseline) and catalyst-treated dye solutions were independently analyzed by an accredited third-party testing laboratory for color, pH, electrical conductivity (EC), and the dye-associated counter-ion species chloride, nitrogen, iodine, and potassium, and the results were benchmarked against the Bureau of Indian Standards drinking-water specification IS 10500:2012. Relative to the untreated baseline, chloride and nitrogen loads in the MV system fell by 18–74% and 36–81%, respectively, depending on the catalyst, while in the RB system, chloride, iodine, and potassium loads fell by 30–71%, 51–87%, and 23–75%, respectively. Electrical conductivity rose in every treated sample, consistent with the release of smaller, more mobile ionic fragments during oxidative breakdown of the parent dye chromophores. A composite ionic-load reduction index (CILRI), defined here as the mean percentage reduction across the measured dye-associated ionic species, ranked rGO–MnO_2 (55.1%) marginally ahead of rGO–CeO_2 (53.8%) and rGO–CuO (51.6%) for MV, and rGO–CuO (70.9%) clearly ahead of rGO–CeO_2 (58.2%), rGO–ZnO (60.0%), and rGO–MnO_2 (46.8%) for RB. Most treated parameters fell within the desirable limits of IS 10500:2012, indicating that rGO–metal oxide photocatalysis can move textile dye wastewater substantially toward potable-quality benchmarks for these specific parameters. However, color readings at or below the instrument quantification limit in both untreated and treated samples, and the absence of direct spectrophotometric dye concentration or catalyst characterization data in this data set, are noted as limitations that warrant follow-up study.

Keywords: rGO; nanocomposite; photocatalysis; dye wastewater; water quality

INTRODUCTION

Synthetic dyes are indispensable to textile processing, yet a substantial fraction of the dye load applied during dyeing and finishing operations is never fixed to the fiber and is discharged with process water [1]. Textile dye effluents are characterized by intense residual color, elevated chemical oxygen demand, variable pH, high total dissolved solids, and the presence of aromatic and heterocyclic dye fragments that resist microbial degradation, so conventional biological treatment trains are frequently insufficient on their own [1], [2]. Beyond their aesthetic impact on receiving water bodies, many textile dyes and their transformation products are reported to be toxic, mutagenic, or otherwise harmful to aquatic organisms and, indirectly, to human health, thereby driving a large and ongoing body of research into advanced treatment alternatives [2].

ISSN No. 2454-6194 | DOI: 10.51584/IJRIAS |Volume XI Issue VII July 2026

Beyond adsorption and biological treatment, textile effluent management more broadly draws on a family of advanced oxidation processes, including ozonation, Fenton and photo-Fenton reactions, electrochemical oxidation, and semiconductor photocatalysis that share the common feature of generating highly reactive oxidizing species in situ to attack recalcitrant organic pollutants that resist conventional biological treatment [2]. Relative to ozonation and electrochemical oxidation, heterogeneous photocatalysis using rGO-supported metal oxides offers a comparatively low-cost, chemically simple route that can in principle be driven by ambient, artificial, or solar light, and the catalyst itself is, in most reported systems, recoverable and reusable over multiple treatment cycles [6], [10], which is an important practical consideration for any treatment technology intended for adoption by resource-constrained textile processing units.

Among these alternatives, heterogeneous semiconductor photocatalysis has attracted sustained attention because it can, in principle, mineralize recalcitrant organic pollutants into simple inorganic end-products using only light, a catalyst, and dissolved oxygen [13], [14]. Under band-gap excitation, a semiconductor photocatalyst generates electron–hole pairs; the photogenerated holes and electrons subsequently react with adsorbed water and oxygen to yield reactive oxygen species such as the hydroxyl radical and the superoxide radical anion, which attack the dye chromophore and its aromatic backbone [13]. A persistent limitation of single-phase metal oxide photocatalysts, however, is the rapid recombination of these photogenerated charge carriers, which caps the achievable quantum efficiency.

Reduced graphene oxide (rGO) has emerged as an effective co-catalyst and charge-carrier scaffold for metal oxide photocatalysts. rGO is typically obtained by oxidative exfoliation of graphite to graphene oxide (GO) using a Hummers-type oxidation, followed by chemical, thermal, or photochemical reduction that partially restores the sp^2 carbon network while retaining a fraction of oxygen-containing surface functionalities [3]. When metal oxide nanoparticles are grown on or anchored to rGO sheets, the resulting two-dimensional conductive scaffold can accept photogenerated electrons from the semiconductor, suppressing electron–hole recombination. At the same time, its large surface area and π-conjugated basal plane provide additional adsorption sites for dye molecules before their oxidative breakdown [4]. This synergy has been documented for a wide range of rGO–metal oxide pairings and dye systems, including rGO–CeO_2 [6], [7], rGO–CuO [8], rGO–Mn_3O_4/MnO_2 [9], rGO–ZnO [10], and rGO–TiO_2 [11] composites, several of which report degradation efficiencies exceeding 90% for cationic and anionic dyes, including methylene blue, indigo carmine, crystal violet, and rhodamine B under UV, visible, or natural-sunlight irradiation.

Cerium oxide (CeO_2) is attractive as a photocatalytic component because of its variable Ce^{3+}/Ce^{4+} oxidation states, associated oxygen-vacancy chemistry, and reasonable UV activity; anchoring CeO_2 nanoparticles on rGO has been shown to narrow the effective optical band gap and improve visible-light response relative to bare CeO_2 [6]. Copper oxide (CuO) offers a narrow band gap and low cost, and CuO/rGO composites have demonstrated enhanced methylene-blue degradation relative to bare CuO [12]. Manganese oxide phases (Mn_3O_4, MnO_2) combine multiple accessible oxidation states with intrinsic redox activity and have been coupled to rGO for both supercapacitor and photocatalytic dye-degradation applications [9]. Zinc oxide (ZnO) is one of the most widely studied UV-active photocatalysts, and ZnO–rGO and related heterostructures have repeatedly shown improved charge separation and dye removal relative to bare ZnO [10]. The present author's prior work on an rGO–La_2O_3 nanocomposite for Congo Red degradation is part of the same line of inquiry into rGO-supported metal-oxide photocatalysts for textile dye removal [5].

Methyl Violet (MV) is a cationic triarylmethane dye widely used in textile dyeing and printing; because of its persistence and reported toxicity toward aquatic organisms, it has been used as a model cationic pollutant in a range of photocatalytic degradation studies on rGO- and metal-oxide-based composites, alongside structurally related triarylmethane dyes such as crystal violet [21]. Rose Bengal (RB) is an anionic xanthene dye used in textiles, food coloring, and photodynamic applications; it has been reported to be toxic to aquatic organisms and epithelial tissues and has likewise served as a model anionic pollutant in heterogeneous photocatalysis research [9], [10].

Most published photocatalytic dye-degradation studies quantify performance through spectrophotometric decolorization and pseudo-first-order kinetic parameters. The present study instead evaluates a complementary and practically important question for treated-effluent management: after batch photocatalytic treatment with

ISSN No. 2454-6194 | DOI: 10.51584/IJRIAS |Volume XI Issue VII July 2026

each of four rGO/metal oxide composites, how does the treated dye solution compare with the physicochemical parameters specified for potable water under the Bureau of Indian Standards specification IS 10500:2012 [12] Untreated MV and RB dye solutions and their corresponding catalyst-treated counterparts were independently analysed by an accredited testing laboratory for colour, pH, electrical conductivity, and the dye-associated counter-ion species chloride, nitrogen, iodine, and potassium. This water-quality-compliance framing complements the conventional decolorization/kinetics literature summarised above and is intended to provide a practically interpretable picture of how far rGO–metal oxide photocatalysis moves a real dye effluent toward a recognized potability benchmark for these specific parameters.

MATERIALS AND METHODS

Chemicals Used

All chemicals used in this study were of analytical reagent (AR) grade (99% purity) and were used as received without any further purification or modification. The chemicals included cerium (III) nitrate hexahydrate, copper nitrate, zinc nitrate, manganese nitrate, trisodium citrate, sodium sulfite, sodium hydroxide, ethanol (alcohol), and deionized water. All reagents were procured from Merck, Bengaluru, India.

Preparation of green fuel

Fresh leaves of lemongrass (*Cymbopogon citratus*) and Ashwagandha (*Withania somnifera*) were collected and thoroughly washed with distilled water to remove dust and other surface impurities. The cleaned leaves were then dried under natural sunlight for 3–4 days until all moisture was removed. The dried leaves were finely ground into a homogeneous powder using a grinder. The resulting leaf powder was subsequently used as a natural biofuel for the solution-combustion synthesis of metal oxide nanomaterials.

Green Synthesis of Metal Oxides Using Green Fuels

Metal oxide nanoparticles were synthesized by the solution combustion method using plant-derived green fuels. Briefly, 3 g of the respective metal nitrate precursor was dissolved in approximately 10 mL of deionized (DI) water in a 100 mL porcelain crucible to obtain a homogeneous precursor solution. Subsequently, 1.5 g of powdered green fuel (lemongrass or *Withania somnifera* (Ashwagandha) leaf powder) was added to the solution and mixed thoroughly to form a uniform paste.

The crucible containing the reaction mixture was then placed in a preheated muffle furnace maintained at 650 °C and heated for 1 h. During combustion, the organic constituents of the green fuel served as reducing and complexing agents, thereby facilitating the rapid formation of porous metal oxide nanoparticles. After completion of the combustion reaction, the crucible was allowed to cool naturally to room temperature for approximately 1 h. The resulting product was collected and ground into a fine powder using an agate mortar and pestle to obtain homogeneous metal oxide nanoparticles.

The stoichiometric ratio of the metal nitrate precursor and the green fuel was determined using the standard propellant chemistry (oxidizer–fuel balance) approach to ensure complete combustion and the formation of phase-pure metal oxide nanoparticles.

Reflux synthesis of rGO/Metal oxide nanocomposite

The rGO/metal oxide nanocomposites were synthesized using a simple reflux method. Initially, 300 mg of reduced graphene oxide (rGO) was dispersed in a round-bottom (RB) flask containing an appropriate amount of deionized water and stirred at 400 rpm using a magnetic stirrer equipped with a heating plate to obtain a uniform suspension. Subsequently, 750 mg of the synthesized metal oxide nanoparticles was gradually added, and the mixture was continuously stirred for 40 min to ensure a homogeneous dispersion and effective interaction between the rGO sheets and the metal oxide particles.

ISSN No. 2454-6194 | DOI: 10.51584/IJRIAS |Volume XI Issue VII July 2026

Thereafter, 2% sodium sulfite and 1.5 g of trisodium citrate were added to the reaction mixture as reducing and stabilizing agents, respectively. The suspension was then refluxed for 1 h under continuous stirring to facilitate the formation of the rGO/metal oxide nanocomposite.

After completion of the reflux process, 50 mL of 3 M sodium hydroxide (NaOH) solution was added slowly as a precipitating agent. The reaction mixture was allowed to cool naturally to room temperature for several hours, after which the supernatant was carefully decanted. The resulting precipitate was collected by filtration using Whatman filter paper (25 mm) and washed several times with ethanol and deionized water to remove residual impurities and unreacted precursors. Finally, the purified product was dried in a hot-air oven at 120 °C for 90 min to obtain the rGO/metal oxide nanocomposite powder.

This procedure was followed for the synthesis of rGO/CeO_2, rGO/CuO, rGO/ZnO, and rGO/MnO_2 nanocomposites under identical experimental conditions.

RESULTS AND DISCUSSION

Baseline characteristics of untreated MV and RB dye solutions

Table 1 summarises the physicochemical characteristics of the untreated MV and RB dye solutions, benchmarked against the desirable limits specified in IS 10500:2012. The untreated MV solution recorded a pH of 7.0, within the IS 10500:2012 desirable band of 5.0–7.0 quoted on that report, an electrical conductivity of 41.62 µS/cm, chloride of 83.95 mg/L (approaching the upper end of the 50–100 mg/L desirable range), and nitrogen of 9.64 mg/L (just below the 10 mg/L limit). The untreated RB solution recorded a pH of 6.2, electrical conductivity of 73.67 µS/cm, iodine of 0.86 mg/L (near the upper end of the <0.1–1 mg/L range), chloride of 79.61 mg/L, and potassium of 7.32 mg/L (below the 10 mg/L limit). Color was reported to be <1.0 Pt–Co units for both untreated dye solutions.

Table 1. Physicochemical characteristics of untreated (baseline) MV and RB dye solutions relative to IS 10500:2012 desirable limits.

Parameter	Unit	MV — untreated	RB — untreated	IS 10500:2012 desirable limit
Colour	Pt–Co units	<1.0	<1.0	Max. 5
pH	—	7.0	6.2	5.0–7.0 / ~6.0–6.8*
Electrical conductivity	µS/cm	41.62	73.67	10–100
Chloride, as Cl^-	mg/L	83.95	79.61	50–100
Nitrogen, as N	mg/L	9.64	—	<10
Iodine, as I	mg/L	—	0.86	<0.1–1
Potassium, as K	mg/L	—	7.32	<10

It is notable that even before any catalytic treatment, the untreated MV and RB dye solutions were already close to several desirable limits in IS 10500:2012 for the parameters measured here (chloride in both dyes, nitrogen in MV, iodine in RB). This baseline proximity to the standard means that the treatment effect reported in Sections 3.2 and 3.3 should be read as a further, catalyst-driven improvement on an already comparatively dilute model dye solution, rather than as evidence that the composites can bring a highly concentrated, industrial-strength textile effluent into compliance from a much more contaminated starting point; the latter would require testing on real, undiluted effluent, as noted in Section 5.

ISSN No. 2454-6194 | DOI: 10.51584/IJRIAS |Volume XI Issue VII July 2026

Effect of rGO–metal oxide composites on MV dye solution quality

Table 2 reports the post-treatment water-quality parameters for the MV dye system across the four catalysts. Relative to the untreated baseline, chloride fell from 83.95 mg/L to between 21.86 mg/L (rGO–MnO_2) and 68.73 mg/L (rGO–ZnO), corresponding to reductions of 73.96%, 56.50%, 48.64%, and 18.13% for rGO–MnO_2, rGO–CuO, rGO–CeO_2, and rGO–ZnO, respectively. Nitrogen fell from 9.64 mg/L to between 1.86 mg/L (rGO–ZnO) and 6.15 mg/L (rGO–MnO_2), corresponding to reductions of 80.71%, 58.92%, 46.78%, and 36.20% for rGO–ZnO, rGO–CeO_2, rGO–CuO, and rGO–MnO_2, respectively. Notably, the catalyst that most reduced chloride (rGO–MnO_2) was not the one that most reduced nitrogen (rGO–ZnO), indicating that the four composites differ in which dye-associated ionic species they most effectively remove or transform, rather than one composite dominating uniformly across all measured parameters.

Electrical conductivity increased in every treated MV sample relative to the untreated baseline, rising from 41.62 µS/cm to between 77.45 µS/cm (rGO–CuO, +86.1%) and 94.76 µS/cm (rGO–ZnO, +127.7%). pH shifted modestly from the untreated value of 7.0 to between 6.35 (rGO–ZnO) and 6.91 (rGO–MnO_2), remaining within or close to the IS 10500:2012 desirable band in all cases.

Table 2. Post-treatment water-quality parameters of MV dye solution for each rGO–metal oxide catalyst.

Parameter	**Unit**	**Untreated**	**rGO–CeO_2**	**rGO–CuO**	**rGO–MnO_2**	**rGO–ZnO**
Colour	Pt–Co units	<1.0	<1.0	<1.0	<1.0	<1.0
pH	—	7.0	6.8	6.4	6.91	6.35
Electrical conductivity	µS/cm	41.62	91.76	77.45	89.67	94.76
Chloride, as Cl^-	mg/L	83.95	43.12	36.52	21.86	68.73
Nitrogen, as N	mg/L	9.64	3.96	5.13	6.15	1.86

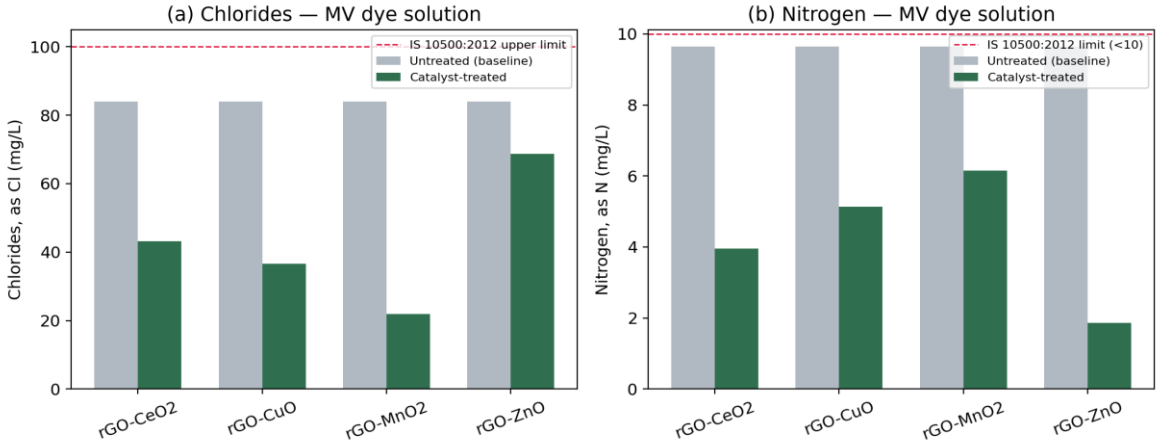

Figure 1. Untreated vs. catalyst-treated (a) chloride and (b) nitrogen concentrations in the MV dye system, with IS 10500:2012 limits shown as dashed reference lines.

Effect of rGO–metal oxide composites on RB dye solution quality

Table 3 reports the post-treatment parameters for the RB dye system. Chloride fell from the untreated 79.61 mg/L to between 23.12 mg/L (rGO–CeO_2) and 55.76 mg/L (rGO–MnO_2), corresponding to reductions of 70.96%, 62.53%, 59.58%, and 29.96% for rGO–CeO_2, rGO–CuO, rGO–ZnO, and rGO–MnO_2, respectively. Iodine fell from 0.86 mg/L to between 0.11 mg/L (rGO–MnO_2) and 0.42 mg/L (rGO–ZnO), corresponding to reductions of 87.21%, 75.58%, 62.79%, and 51.16% for rGO–MnO_2, rGO–CuO, rGO–CeO_2, and rGO–ZnO,

ISSN No. 2454-6194 | DOI: 10.51584/IJRIAS |Volume XI Issue VII July 2026

respectively. Potassium fell from 7.32 mg/L to between 1.86 mg/L (rGO–CuO) and 5.62 mg/L (rGO–MnO_2), corresponding to reductions of 74.59%, 69.13%, 40.71%, and 23.22% for rGO–CuO, rGO–ZnO, rGO–CeO_2, and rGO–MnO_2, respectively. As with the MV system, no single catalyst dominated across all three ionic parameters: rGO–CuO gave the largest potassium and second-largest iodine reductions, rGO–CeO_2 gave the largest chloride reduction, and rGO–MnO_2 gave the largest iodine reduction but the smallest chloride and potassium reductions.

Electrical conductivity again increased after treatment in every case. However, the magnitude of increase was noticeably smaller for RB (+4.4% to +30.6%) than for MV (+86.1% to +127.7%), which may reflect the different counter-ion chemistry of the anionic RB system relative to the cationic MV system. pH values for the treated RB samples (6.09–6.27) remained close to the untreated baseline of 6.2.

Table 3. Post-treatment water-quality parameters of RB dye solution for each rGO–metal oxide catalyst.

Parameter	**Unit**	**Untreated**	**rGO–CuO**	**rGO–MnO_2**	**rGO–ZnO**	**rGO–CeO_2**
Colour	Pt–Co units	<1.0	<1.0	<1.0	<1.0	<1.0
pH	—	6.2	6.12	6.09	6.27	6.1
Electrical conductivity	µS/cm	73.67	76.91	96.23	85.38	78.54
Iodine, as I	mg/L	0.86	0.21	0.11	0.42	0.32
Chloride, as Cl^-	mg/L	79.61	29.83	55.76	32.18	23.12
Potassium, as K	mg/L	7.32	1.86	5.62	2.26	4.34

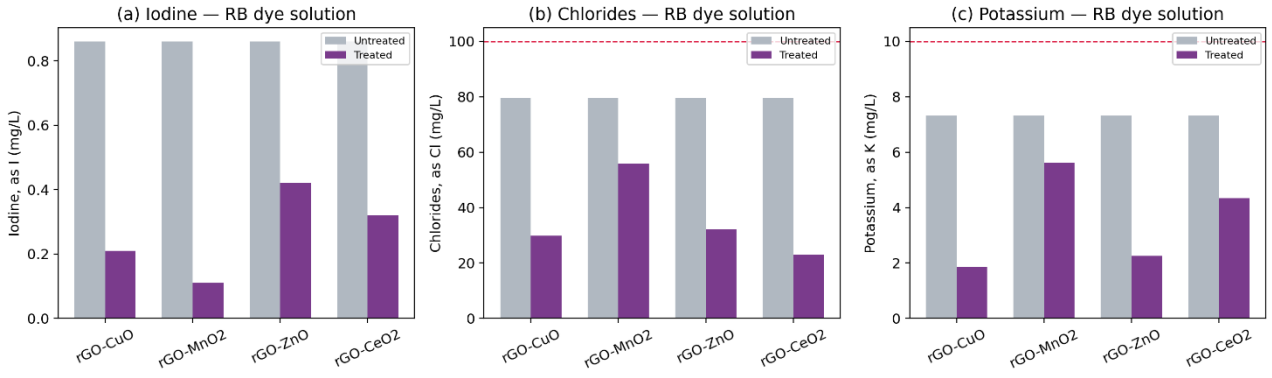

Figure 2. Untreated vs. catalyst-treated (a) iodine, (b) chloride, and (c) potassium concentrations in the RB dye system.

Comparative catalyst performance: composite ionic-load reduction index

The CILRI computed for each catalyst and dye system, as defined in Section 2.5. For the MV system, the four catalysts were closely grouped (49.4–55.1%), with rGO–MnO_2 (55.1%) marginally ahead of rGO–CeO_2 (53.8%), rGO–CuO (51.6%), and rGO–ZnO (49.4%). For the RB system, the spread was wider (46.8–70.9%), with rGO–CuO (70.9%) clearly outperforming rGO–ZnO (60.0%), rGO–CeO_2 (58.2%), and rGO–MnO_2 (46.8%). Two observations follow from this comparison. First, catalyst ranking is not conserved across the two dye systems studied here: rGO–MnO_2 ranked first for MV but last for RB, while rGO–CuO ranked second-to-last for MV but first for RB. This is consistent with the differing adsorption and interfacial chemistry expected for a cationic dye (MV) versus an anionic dye (RB) on a given metal-oxide/rGO surface, where surface charge, isoelectric point, and specific ion affinity of the metal oxide component can be expected to interact differently with each dye's counter-ion population [10]. Second, the between-catalyst spread was narrower for MV than for

ISSN No. 2454-6194 | DOI: 10.51584/IJRIAS |Volume XI Issue VII July 2026

RB, suggesting that catalyst identity was a comparatively weaker driver of the measured ionic-load response for the MV system under the conditions of this study.

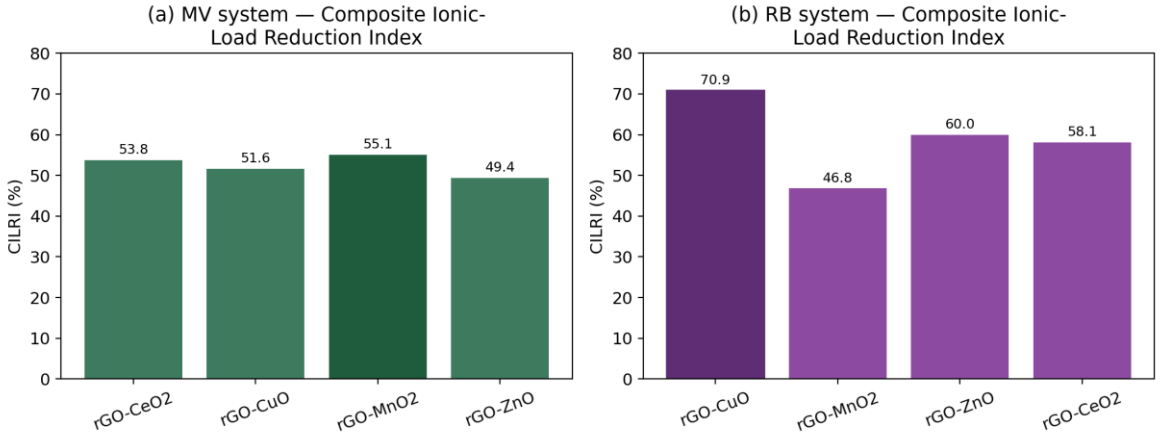

Figure 3. Composite ionic-load reduction index (CILRI) by catalyst for (a) the MV system and (b) the RB system.

Behavior of pH and electrical conductivity

Across both dye systems, electrical conductivity rose after photocatalytic treatment relative to the untreated baseline, even in samples where the specifically measured ionic species (chloride, nitrogen, iodine, potassium) declined. This apparently counter-intuitive pattern is consistent with the general mechanism of oxidative dye mineralisation reported in the photocatalysis literature, in which the parent dye chromophore — a comparatively large, weakly conducting organic cation or anion — is progressively cleaved by hydroxyl and superoxide radical attack into smaller, more mobile inorganic and low-molecular-weight ionic fragments, which contribute more effectively to solution conductivity per unit mass than the intact dye molecule [13], [14]. The pH values of all treated samples, both MV and RB, remained close to neutral and within or near the IS 10500:2012 desirable range, indicating that none of the four catalysts drove the treated solutions toward strongly acidic or alkaline conditions under the conditions tested.

Limitation of the color parameter and comparison with the wider literature

Color, measured on the Pt–Co (Hazen) scale following IS 3025 (Part 4):2021, was reported as below 1.0 Pt–Co units in both the untreated and all catalyst-treated samples for both dyes. Because this value was already at or below the method's reporting resolution in the untreated baseline, the color parameter measured here could not detect any additional decolorization achieved by the four catalysts, and no color-removal claim is made from this data set. This stands in contrast to the wider rGO–metal oxide photocatalysis literature, where degradation is typically followed by UV–visible spectrophotometry at the dye's characteristic absorption maximum, yielding continuous percentage-degradation and pseudo-first-order rate-constant values; reported degradation efficiencies for structurally related cationic and anionic dyes on rGO–metal oxide composites, and on related metal-oxide/rGO and semiconductor photocatalysts more broadly, commonly range from about 85% to above 95% within 60–180 minutes of irradiation [6], [7], [9], [10], [11], [15], [16], [17], [18], [19], [20], [21]. The ionic-species reductions reported in Sections 3.2–3.4 of the present study are a complementary but distinct line of evidence: they reflect changes in the dye-associated counter-ion population of the treated solution rather than a direct measurement of chromophore breakdown, and the two should not be conflated. A parallel spectrophotometric or chemical-oxygen-demand assessment, discussed further in Section 5, would be needed to establish the fractional destruction of the MV and RB chromophores themselves under the conditions used here.

Plausible degradation and ion-removal mechanism

Although catalyst characterization data (XRD, FTIR, UV–DRS, SEM/TEM, BET) were not available for the four composites used in this study, the pattern of ionic-species removal observed here is broadly consistent with the electron-transfer mechanism reported for rGO–metal oxide photocatalysts in the literature. Under illumination, the metal oxide component (CeO_2, CuO, MnO_2, or ZnO) generates electron–hole pairs; the

ISSN No. 2454-6194 | DOI: 10.51584/IJRIAS |Volume XI Issue VII July 2026

conductive rGO scaffold accepts and delocalizes the photogenerated electrons, suppressing charge-carrier recombination, while the valence-band holes and rGO-mediated electrons react with adsorbed water and dissolved oxygen to generate hydroxyl and superoxide radicals [13], [14], [16]. These reactive oxygen species progressively cleave the aromatic and heterocyclic dye structures, releasing smaller ionic and low-molecular-weight fragments into solution, a process consistent with the increase in conductivity and the reduction in the specifically measured counter-ion species (chloride, nitrogen, iodine, potassium) documented in Sections 3.2 and 3.3. The oxygen-containing functional groups retained on partially reduced rGO additionally provide adsorption sites for initially intact, positively or negatively charged dye species, which have been reported to enhance the overall removal efficiency of rGO-supported photocatalysts relative to their unsupported metal oxide counterparts [4], [16].

Comparison with selected rGO–metal oxide dye-degradation studies

Table 4 places the present findings alongside a selection of previously reported rGO–metal oxide dye-degradation studies. Because the present study reports ionic-load reduction and IS 10500:2012 compliance rather than spectrophotometric percentage degradation, the values are not directly numerically comparable to the literature decolorization efficiencies; the table is intended instead to situate the composite systems used here within the broader family of rGO–metal oxide photocatalysts reported for structurally comparable dyes, and to highlight the difference in evaluation metric between this study and the conventional literature.

Table 4. Selected rGO–metal oxide dye-degradation studies compared with the present work.

Photocatalyst system	Dye evaluated	Reported outcome	Source
rGO–CeO_2	Rose Bengal	~95% decolourisation (spectrophotometric), pseudo-first-order kinetics	[7]
rGO–ZnO	Chloramphenicol (model organic pollutant)	Enhanced adsorptional–photocatalytic removal vs. bare ZnO	[10]
CuO/rGO	Methylene Blue	Enhanced catalytic degradation vs. bare CuO	[8]
rGO–Mn_3O_4	Model organic dyes	Enhanced solar-light degradation vs. bare Mn_3O_4	[9]
rGO–TiO_2 (Ag/Fe-doped)	Methylene Blue	Effective visible-light degradation within 150 min	[11]
rGO–La_2O_3 (author's prior work)	Congo Red	Degradation of 10 ppm dye within 65 min	[5]
rGO–CeO_2/CuO/MnO_2/ZnO (this study)	Methyl Violet, Rose Bengal	18–81% reduction in dye-associated ionic species; most treated parameters within IS 10500:2012 desirable limits	Present study

Practical implications for textile effluent management

From an effluent-management perspective, the practical question is not only how much of the dye chromophore is destroyed, but also whether the treated stream approaches parameters that would allow safer discharge or downstream reuse. The present results indicate that batch treatment with any of the four rGO–metal oxide composites moved both the MV and RB systems toward, and in several parameters within, the IS 10500:2012 desirable limits for pH, and reduced the chloride, nitrogen, iodine, and potassium loads associated with the dye and its counter-ions, in most cases substantially. The consistent rise in electrical conductivity after treatment is

ISSN No. 2454-6194 | DOI: 10.51584/IJRIAS |Volume XI Issue VII July 2026

a practically relevant caveat: while it is consistent with oxidative fragmentation of the parent dye, it also means that conductivity alone should not be used as a proxy for "cleaner" water in this type of treatment train, and should instead be interpreted alongside the ionic-species data and, ideally, a direct measure of residual organic content such as chemical oxygen demand. Because catalyst ranking was not conserved between the cationic MV and anionic RB systems (Section 3.4), a practical treatment train handling mixed or variable dye effluent streams may benefit from either a catalyst blend or a staged treatment approach, rather than a single catalyst optimized for a single dye class.

CONCLUSION

Four reduced graphene oxide–metal oxide nanocomposites (rGO–CeO_2, rGO–CuO, rGO–MnO_2, rGO–ZnO) were evaluated for their effect on the post-treatment water quality of two structurally distinct textile dyes, cationic Methyl Violet and anionic Rose Bengal, relative to untreated baselines and the IS 10500:2012 potable-water specification. Photocatalytic treatment reduced the dye-associated ionic load of chloride and nitrogen for MV, and chloride, iodine, and potassium for RB by 18–81%, depending on catalyst and species. At the same time, electrical conductivity increased in every treated sample, consistent with oxidative fragmentation of the parent dye structures into smaller, more mobile ionic species. A composite ionic-load reduction index indicated rGO–MnO_2 as the most effective catalyst for the MV system and rGO–CuO as the most effective for the RB system, with no catalyst dominating uniformly across both dye systems, underscoring that catalyst selection for a given textile effluent stream should account for the specific dye chemistry involved rather than assuming transferability of performance across dye classes. Treated pH, and in most cases treated conductivity, chloride, nitrogen, iodine, and potassium, fell within or close to IS 10500:2012 desirable limits, indicating that rGO–metal oxide photocatalysis can move textile dye wastewater substantially toward recognized potable-water benchmarks on these specific parameters.

Limitations and Future Scope

The present study successfully demonstrated the green synthesis, characterization, and application of reduced graphene oxide (rGO)-metal oxide (CeO_2, CuO, MnO_2, and ZnO) nanocomposites for the photocatalytic degradation of organic dyes and the improvement of wastewater quality. However, the investigation was limited to laboratory-scale experiments using selected model dyes (Methyl Violet and Rose Bengal) and wastewater samples under controlled conditions. The photocatalytic performance under real industrial operating conditions, natural sunlight, and continuous-flow systems was not evaluated. Furthermore, only selected physicochemical parameters were analyzed, while the identification of degradation intermediates, long-term catalyst stability, large-scale synthesis, economic feasibility, and comprehensive environmental impact assessments were beyond the scope of this study. In particular, this study did not include direct UV–visible spectrophotometric monitoring of dye concentration and associated pseudo-first-order kinetics, phytochemical characterization (e.g., total phenolic content, antioxidant activity) of the lemongrass and Ashwagandha green-fuel extracts to clarify their reducing/capping role, multi-cycle reusability and stability testing of the four rGO–metal oxide composites, or a catalyst-free, light-only control experiment to isolate the photocatalytic contribution from photolysis; each of these is identified here as a specific, named objective for the planned follow-up study. Future research should focus on scaling up the green synthesis process, evaluating the catalysts in pilot-scale and industrial wastewater treatment systems, and investigating their effectiveness against a wider range of emerging contaminants such as pharmaceuticals, pesticides, and heavy metals. In addition, the development of advanced heterojunction and magnetic nanocomposites with improved visible-light activity, enhanced recyclability, and greater stability should be explored. Detailed toxicity studies, life-cycle assessment, techno-economic analysis, and the design of efficient continuous-flow photocatalytic reactors will further support the practical implementation of these nanocomposites. Overall, the findings of this research provide a strong foundation for developing sustainable, environmentally friendly, and high-performance photocatalytic materials for future wastewater treatment and water reuse applications.

Author Contributions: Roopa M C: conceptualization, methodology, writing original draft, **Sharadadevi Kallimani:** review and editing. **Umadevi K M:** sample coordination, formal analysis; **Shilpa P Raikar:** formal analysis, data curation.

ACKNOWLEDGMENTS

Department of Environmental Science, Davangere University, Davangere.

Conflict of Interest: The authors declare no conflict of interest.

REFERENCES

1. Yaseen, D. A., & Scholz, M. (2019). Textile dye wastewater characteristics and constituents of synthetic effluents: A critical review. International Journal of Environmental Science and Technology, 16(2), 1193–1226.
2. Al-Tohamy, R., Ali, S. S., Li, F., Okasha, K. M., Mahmoud, Y. A.-G., Elsamahy, T., Jiao, H., Fu, Y., & Sun, J. (2022). A critical review on the treatment of dye-containing wastewater: Ecotoxicological and health concerns of textile dyes and possible remediation approaches for environmental safety. Ecotoxicology and Environmental Safety, 231, Article 113160.
3. Hummers, W. S., & Offeman, R. E. (1958). Preparation of graphitic oxide. Journal of the American Chemical Society, 80(6), 1339.
4. Habte, A. T., & Ayele, D. W. (2019). Synthesis and characterization of reduced graphene oxide (rGO) started from graphene oxide (GO) using the Tour method with different parameters. Advances in Materials Science and Engineering, 2019, Article 5058163.
5. Mylarappa, M., Selvam, C., Sanjeevappa, H. K., Prasanna Kumar, S. G., Krishnamurthy, G., & Muttanagoud, K. N. (2024). Reduced graphene oxide loaded La2O3 nanocomposite for dye degradation and antioxidant studies. Results in Surfaces and Interfaces, 14, Article 100202.
6. Rajendran, R., Shrestha, L. K., Minami, K., Subramanian, M., Jayavel, R., & Ariga, K. (2014). Dimensionally integrated nanoarchitectonics for a novel composite from 0D, 1D, and 2D nanomaterials: RGO/CNT/CeO2 ternary nanocomposites with electrochemical performance. Journal of Materials Chemistry A, 2(43), 18480–18487.
7. Kumar, S., Ojha, A. K., et al. (2016). One-step in situ synthesis of CeO2 nanoparticles grown on reduced graphene oxide as an excellent fluorescent and photocatalyst material under sunlight irradiation. Physical Chemistry Chemical Physics, 18, 11157–11167.
8. Prasad, G., Tamang, S., Biswas, J., Jha, S., & Bhattacharyya, N. K. (2025). A novel CuO/rGO composite for catalytic degradation of methylene blue. Next Materials.
9. Ghosh, S., Basu, S., & Baskey (Sen), M. (2017). Decorating mechanism of Mn3O4 nanoparticles on reduced graphene oxide surface through reflux condensation method to improve photocatalytic performance. Journal of Materials Science: Materials in Electronics, 28, 17860–17870.
10. Sodeinde, K. O., Olusanya, S. O., Lawal, O. S., Sriariyanun, M., & Adediran, A. A. (2022). Enhanced adsorptional-photocatalytic degradation of chloramphenicol by reduced graphene oxide–zinc oxide nanocomposite. Scientific Reports, 12, Article 17054.
11. Jaihindh, D. P., Chen, C.-C., & Fu, Y.-P. (2018). Reduced graphene oxide-supported Ag-loaded Fe-doped TiO2 for the degradation mechanism of methylene blue and its electrochemical properties. RSC Advances, 8, 6079–6091.
12. Bureau of Indian Standards. (2012). Indian standard: Drinking water — Specification (2nd revision) (IS 10500:2012). BIS.
13. Hoffmann, M. R., Martin, S. T., Choi, W., & Bahnemann, D. W. (1995). Environmental applications of semiconductor photocatalysis. Chemical Reviews, 95(1), 69–96.
14. Mills, A., & Le Hunte, S. (1997). An overview of semiconductor photocatalysis. Journal of Photochemistry and Photobiology A: Chemistry, 108(1), 1–35.
15. Shabil Sha, M., Anwar, H., Musthafa, F. N., Al-Lohedan, H., Alfarwati, S., Rajabathar, J. R., Alahmad, J. K., Cabibihan, J.-J., Karnan, M., & Sadasivuni, K. K. (2024). Photocatalytic degradation of organic dyes using reduced graphene oxide (rGO). Scientific Reports, 14, Article 3608.
16. Er Siong, V. L., Lee, K. M., Juan, J. C., Lai, C. W., Tai, X. H., & Khe, C. S. (2019). Removal of methylene blue dye by solvothermally reduced graphene oxide: A metal-free adsorption and photodegradation method. RSC Advances, 9, 37686–37695.

ISSN No. 2454-6194 | DOI: 10.51584/IJRIAS |Volume XI Issue VII July 2026

17. Parthipan, P., Cheng, L., Rajasekar, A., Govarthanan, M., & Subramania, A. (2021). Biologically reduced graphene oxide as a green and easily available photocatalyst for degradation of organic dyes. Environmental Research, 196, Article 110983.
18. Yu, L., Xu, W., Liu, H., & Bao, Y. (2022). Titanium dioxide–reduced graphene oxide composites for photocatalytic degradation of dyes in water. Catalysts, 12(11), Article 1340.
19. Ziyaadini, M., & Ghashang, M. (2021). Sunlight-induced photocatalytic degradation of indigo carmine using Bi5Ti3FeO15 layered structure. Optik, 228, Article 166207.
20. Wang, J., Zhu, H., Hurren, C., Zhao, J., Pakdel, E., Li, Z., & Wang, X. (2015). Degradation of organic dyes by P25-reduced graphene oxide: Influence of inorganic salts and surfactants. Journal of Environmental Chemical Engineering, 3(2), 1437–1443.
21. Al-Ansari, S. H., Gomaa, H., Abdel-Rahim, R. D., Ali, G. A. M., & Nagiub, A. M. (2024). Recycled gold-reduced graphene oxide nanocomposite for efficient adsorption and photocatalytic degradation of crystal violet. Scientific Reports, 14, Article 4386.